On the effectiveness of Leverett approach for describing the water transport in fuel cell diffusion media

E.C. Kumbur, K.V. Sharp, M.M. Mench *

*Fuel Cell Dynamics and Diagnostics Laboratory, Department of Mechanical and Nuclear Engineering,
The Pennsylvania State University, University Park, PA 16802, United States*

Abstract

This paper investigates the effectiveness of employing the traditional Leverett approach for describing the capillary-induced flow in thin-film fuel cell diffusion media (DM) *with mixed wettability*. A one-dimensional steady-state analytical model is developed to analyze the capillary transport of liquid water through the thin-film DM. A capillary pressure–liquid saturation relation is derived based on the experimental data reported by Gostick et al. [J.T. Gostick, M.W. Fowler, M.A. Ioannidis, M.D. Pritzker, Y.M. Volfkovich, A. Sakars, J. Power Sources, 156 (2006) 375]. The empirical fit is applicable to the fuel cell DMs tested by reference [J.T. Gostick, M.W. Fowler, M.A. Ioannidis, M.D. Pritzker, Y.M. Volfkovich, A. Sakars, J. Power Sources, 156 (2006) 375] under a limited set of conditions, providing a means to evaluate the effectiveness of the traditional Leverett approach. Furthermore, a new characteristic relative permeability correlation appropriate for the tested DMs under the given conditions was obtained by fitting the experimental capillary pressure data [J.T. Gostick, M.W. Fowler, M.A. Ioannidis, M.D. Pritzker, Y.M. Volfkovich, A. Sakars, J. Power Sources, 156 (2006) 375] into four well-established empirical models. The empirically-derived relationships are then integrated into an analytical model framework in order to compare the liquid saturation profiles predicted by both approaches. The results show that use of the standard Leverett approach equipped with Leverett *J*-function can lead to significant errors; therefore, an extension of this approach appropriate for fuel cell DM with *mixed wettability* is needed for reliable model predictions. Finally, a sensitivity analysis is performed to assess the relative significance of the various input parameters on the predicted saturation profiles.
© 2007 Elsevier B.V. All rights reserved.

Keywords: Capillary flow; Gas diffusion layer; Leverett; Polymer electrolyte fuel cell; Two-phase flow; Water management

1. Introduction

The efficient operation of polymer electrolyte fuel cells (PEFCs) requires complex water management strategies [1–5] due to the interaction of electrochemistry, material science, and transport phenomena. Reliable and efficient operation requires a delicate balance between membrane hydration and the avoidance of cathode flooding. Adequate water in the membrane electrolyte and catalyst layers is important for achieving suitable performance. However, the presence of excess liquid water in the diffusion media (DM), catalyst layer and the flow channel increases the reactant transport resistance to the electrode cata-

lyst surface, causing severe performance loss. The existence of two-phase flow in the porous DM presents a major bottleneck in the design optimization of PEFCs due to the highly interrelated and ill-defined transport phenomena involved.

Because of the minute length scales and presumed anisotropic nature of the thin-film DM, the multi-phase transport behavior inside the DM is not yet fully understood. Within the DM, gravitational and viscous forces are relatively small compared to capillary forces [5]. Hence, two-phase transport in the DM is primarily controlled by capillary action. The pressure difference arising from the interfacial tensions at the liquid–gas interface front is referred to as the capillary pressure. The capillary pressure is a strong function of liquid saturation (s_l) which is a key parameter representing the available pore space, through which reactant gases can diffuse.

Fuel cell performance is known to exhibit hysteresis, for a variety of reasons, but often because of liquid water motion. Many studies [5–9] reveal that liquid water transport is a dom-

Nomenclature

F	Faraday constant (96,485 C (eq mol)$^{-1}$)
I	current density (A cm^{-2})
k	permeability (m^{-2})
k_r	relative permeability (unitless)
m	fitting parameter (unitless)
MW	molecular weight (g mol^{-1})
P	pressure (Pa)
s	liquid saturation (unitless)
u	phase velocity in x direction (m s^{-1})
x	distance, m
v	phase velocity (m s^{-1})

Greek letters

α	net water transfer coefficient (unitless)
ε	porosity (unitless)
γ	surface tension of water–air (N m^{-1})
λ	pore distribution index (unitless)
μ	absolute viscosity (kg m s^{-1})
ν	kinematic viscosity of water (m^2 s^{-1})
θ	contact angle (°)
ρ	density (kg m^{-3})

Subscripts

C	capillary
e	effective
g	gas
int	interface
irr	irreducible
l	liquid
w	wetting phase
nw	non-wetting phase

inating factor influencing the performance of the fuel cell, and is closely related to the liquid saturation distribution in DM. Therefore, accurate prediction of the liquid water distribution in the DM as a function of material properties is of great interest to understand the capillary transport phenomenon in the DM [6–11]. An extensive review of the recent modeling efforts is provided in Ref. [12]. Since the vast majority of the background work on defining the capillary pressure–saturation relation has been performed in the soil science and oil extraction fields, a generic Leverett approach from soil science has been commonly employed to represent the water transport or retention behavior of the fuel cell DM as a first step toward achieving an accurate two-phase transport model for fuel cells studies [5–7]. The Leverett approach, indeed, is viewed as an indispensable tool for many modelers and serves as a useful starting point to model the liquid transport in the porous diffusion media. Although the usefulness of the Leverett approach is clear, the degree of the applicability of the traditional Leverett approach *in its original form* to the highly anisotropic thin-film DM has not been conclusively established. Since the naturally hydrophilic fuel cell DM material itself is impregnated with an *anisotropic* coating

of hydrophobic material (PTFE or other), it yields a complex bi-modal pore size distribution with *mixed wettability*, complicating the transport phenomena therein.

Specific concerns center around the characteristic morphological differences in fuel cell DM and conditions under which the Leverett approach equipped with *J*-function was derived, including the fact that it was: empirically derived to simulate a range of common soils with *uniform wettability*, ignoring the observed hysteresis in porous media and most importantly, developed for isotropic soil beds with a high volume to surface area ratio [13]. As a result of the anisotropic coating of hydrophobic material (PTFE or other), the liquid water can be *both* the wetting (on untreated DM fiber), and non-wetting phase (on PTFE coated fiber) phase [12], complicating the mathematical description of the transport phenomena. Furthermore, the definition of contact angle representing the wettability characteristics of the anisotropic DM with mixed wettability is typically taken as a statistical average over the entire medium, obscuring local effects which may differ from the whole. Therefore, the applicability of the traditional Leverett approach to thin-film fuel cell DM is questionable, and is the focus of this paper.

Another important parameter governing the capillary transport inside the DM is relative permeability, which is also a strong function of liquid saturation. In PEFC modeling studies, a typical relative permeability expression for non-consolidated sands is adapted to describe the phase transport in DM due to its simplicity, that is:

$$k_{r-nw} = s_{nw}^3 \tag{1}$$

where k_{r-nw} and s_{nw} represent the relative permeability of non-wetting phase and non-wetting saturation, respectively. However, the applicability of this correlation to the thin-film DM is also questionable and yet unproven. Direct experimental evidence is still needed to verify the applicability of these empirical correlations, since the reliability of the computational output is directly related to the quality of the input parameters.

The direct measurement of liquid saturation distribution through the pores of the DM is an experimental challenge and only limited experimental studies are yet available in the open literature [1,2]. Recently, Gostick et al. [10] reported a novel experimental approach for determining the dependence of capillary pressure on wetting phase saturation along a desaturation path (drainage) for various DMs. This technique, the method of standard porosimetry (MSP), is capable of distinguishing the hydrophilic pore distribution from the total pore network, unlike mercury intrusion porosimetry. Using standard porosimetry, Gostick et al. [10] measured the static capillary pressure as a function of saturation during the drainage process for a certain PEFC DM materials under a limited set of conditions.

The present study reports a detailed comparative analysis of the constitutive relations[1] relations describing the capillary-induced flow in fuel cell DM, particularly focusing on the applicability of the commonly employed standard Leverett

---

[1] The term constitutive relation is used here to denote the empirical relation of capillary pressure and liquid saturation in a fuel cell diffusion media.
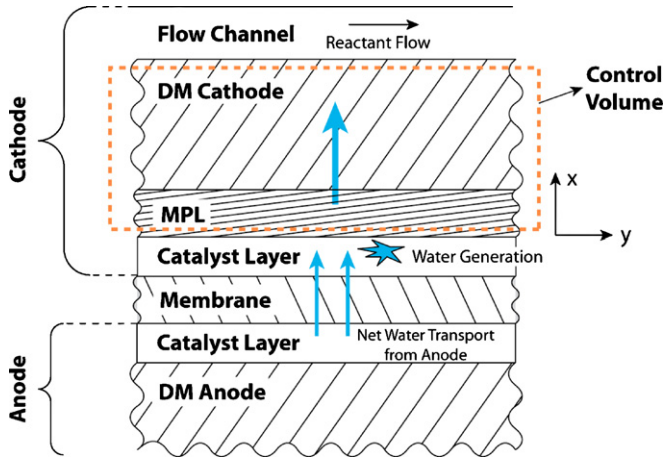
Fig. 1. Schematic of control volume.

approach to thin-film fuel cell DM with *mixed wettability*. The saturation prediction of the Leverett approach in *its original form* (as applied to the most fuel cell models) was compared with the prediction of the empirical capillary pressure–saturation correlation derived from the experimental data provided by Ref. [10]. The reasons underlying the variations in liquid saturation predictions within the DM were linked to the prediction potential of the Leverett approach. With the aid of these analyses, the ineffectiveness of employing Leverett approach in *its original form* is discussed and the necessity of development of a modified Leverett approach appropriate for thin-film fuel cell media is addressed.

2. Theoretical

2.1. Theoretical analysis of liquid transport through DM

A basic analytical model describing the capillary liquid flow has been developed to predict the liquid saturation distribution inside the DM. This model is constructed to provide a tool to assess the saturation predictions of the constitutive relations while isolating all other effects, including: humidity, 2D effects, inlet cell conditions and time dependent parameters, etc. Fig. 1 shows a schematic of the chosen control volume in the fuel cell. In the present model, the liquid water flowing inside the DM is assumed to be Newtonian and incompressible, and the flow in the pores of the DM is presumed to be uni-directional, steady and laminar.

In the steady state, once the gas phase is fully saturated with water vapor, assuming evaporation and condensation do not take place in the DM, liquid water flow becomes the only mode of

$$
J(s_l) = \begin{cases} 1.417(1 - s_l) - 2.120(1 - s_l)^2 + 1.263(1 - s_l)^3 & \text{if } \theta < 90° \Rightarrow \text{Hydrophilic} \\ 1.417 s_l - 2.120 s_l^2 + 1.263 s_l^3 & \text{if } \theta > 90° \Rightarrow \text{Hydrophobic} \end{cases} \tag{5}
$$

the water transport across the DM [6]. Water generation in the catalyst layer, water transport across the membrane, and condensation or evaporation within the DM pores cause non-uniformity in the saturation distribution. As hydrophobic DM pores are
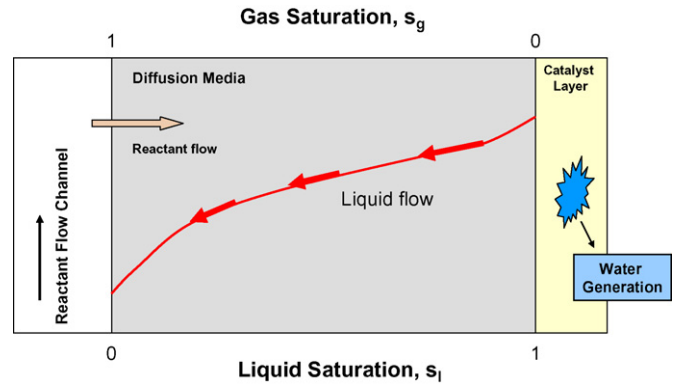

Fig. 2. Illustration of capillary-induced liquid flow in a fuel cell DM.

filled by the liquid water, the liquid phase pressure increases, eventually driving the liquid water from higher to lower liquid pressure regions. As a result, the liquid water in the DM is driven *via* capillary action produced by the liquid saturation gradients in DM. This phenomenon is illustrated in Fig. 2.

In a hydrophobic DM, capillary pressure is defined as the difference between liquid pressure (non-wetting phase) and reactant gas pressure (wetting phase).

$$
P_C = P_l - P_g \tag{2}
$$

The liquid flow through the porous DM can be described by Darcy's law. Darcy's law relates the flow rate through a porous medium to the pressure gradient across the porous media and the permeability of the porous media. Assuming constant gas phase pressure ($P_g \approx$ const) and no convective gas flow, the governing liquid transport equation in the porous DM can be expressed as:

$$
\vec{v}_l = \frac{-k\,k_r}{\mu}\vec{\nabla}P_C \quad \text{where } \vec{\nabla}P_C \approx \vec{\nabla}P_l \tag{3}
$$

where k is absolute permeability of the porous media, k_r the fluid relative permeability, μ the absolute viscosity of the fluid and $\vec{v}_l$ is the velocity of the flowing fluid.

A generic Leverett approach has been commonly employed to describe the capillary pressure–saturation relation of the DM in two-phase PEFC models. Leverett [21] related capillary pressure to saturation in porous media by:

$$
P_C = \gamma\,\cos\theta\left(\frac{\varepsilon}{k}\right)^{1/2}J(s_l) \tag{4}
$$

where k, ε, θ, γ and $J(s_l)$ represent the gas phase or liquid absolute permeability, porosity of the DM, contact angle between liquid–solid phase, surface tension and the Leverett function in terms of liquid saturation, respectively. The standard Leverett function, $J(s_l)$, is given as [21]:

The liquid pressure (P_l) is a function of local liquid saturation; hence, the capillary pressure gradient can be expressed as:

$$
\vec{\nabla}P_l \approx \vec{\nabla}P_C = \gamma\,\cos\theta\sqrt{\frac{\varepsilon}{k}}\left(\frac{dJ}{ds_l}\right)\vec{\nabla}s_l \tag{6}
$$

Inserting Eq. (6) into Eq. (3), the governing equation yields:

$$\vec{v}_l = \frac{k\,k_r}{\mu_l}\gamma\cos\theta\sqrt{\frac{\varepsilon}{k}}\left(\frac{dJ}{ds_l}\right)\vec{\nabla}s_l \tag{7}$$

Assuming all the water produced by electrochemical reaction in a PEFC is in liquid form, the mass flux of liquid water going into the cathode DM is equal to sum of the net water transport from the anode side and the amount of water generated in the catalyst layer due to the electro-chemical reaction. The net water flux across the membrane from anode to cathode can be characterized by a net water transport coefficient, α [29]. Combining the net water transport with the water production, the net water flux to the cathode DM yields:

$$\rho_l v_l = \frac{I}{2F}(2\alpha + 1)MW^{H_2O} \tag{8}$$

where MW^{H_2O} is the molecular weight of the water, α the net water transport coefficient to the cathode DM, I the current density and F is the Faradic constant (96,485 C mol eq^{-1}). Assuming one-dimensional flow, substituting Eq. (8) into Eq. (7), the final form of the governing equation becomes:

$$\frac{I(2\alpha+1)MW^{H_2O}\mu_l}{2F\gamma\rho_l\cos\theta\sqrt{k\varepsilon}} = -k_r\frac{dJ}{ds_l}\frac{ds_l}{dx} \tag{9}$$

This relationship describes the steady-state liquid water transport across the fuel cell DM. As seen from Eq. (9), the operational conditions and DM material properties are coupled with the fluid properties and the mass transport rate are explicitly linked to the liquid saturation.

2.1.1. Micro-porous layer interface

Generally, the cathode side of PEFC consists of a coarse DM and a finer micro-porous layer (MPL), both of which are generally classified as hydrophobic, based on surface contact angle. However, the DM is actually a *mixed wettability* network, since the base material of carbon-fiber is hydrophilic. Micro-porous layers are introduced between the DM and catalyst layer (CL) to provide better membrane electrical contact and improve the water management. The liquid water transport of the MPL is governed by capillary action. In equilibrium, the capillary pressure across the interface between the DM and MPL is continuous. The different material properties of these two layers cause a discontinuity in the liquid saturation across the interface [7], as illustrated in Fig. 3. The magnitude of the discontinuity or the jump in the saturation at the interface strongly depends on the material properties of these two layers, specifically the hydrophobicity and pore radius. Imposing the capillary pressure balance at the interface yields:

$$P_C^{DM}\big| = P_C^{MPL}\big|_{DM-MPL\ \text{Interface}}$$

$$\cos\theta_{MPL}\left(\frac{\varepsilon_{MPL}}{k_{MPL}}\right)^{1/2}J(s_{l-int}^{MPL}) = \cos\theta_{DM}\left(\frac{\varepsilon_{DM}}{k_{DM}}\right)^{1/2}J(s_{l-int}^{DM}) \tag{10}$$

With a known liquid saturation at the DM interface, the equilibrium MPL liquid saturation at the interface can be calculated
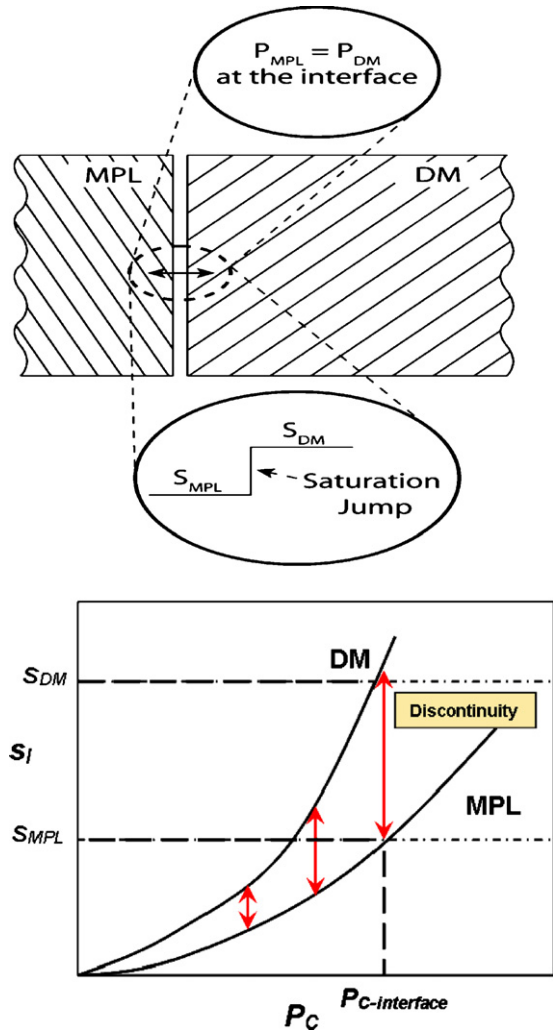

Fig. 3. Boundary conditions and saturation jump at the interface of the DM and MPL.

from Eq. (10). Since the structural characteristics of MPL and physics of the flow through the MPL are similar to the DM, the governing equation (Eq. (9)) can also be applied to the MPL in order to map the saturation distribution profile inside the MPL.

2.2. Constitutive equations

2.2.1. Relative permeability

When two or more fluids are present in the porous media, an additional parameter, known as relative permeability, is used to represent the ability of the porous media to conduct various fluids simultaneously. Relative permeability is defined as the ratio of the effective permeability of one fluid to the absolute permeability of the porous media [13,14]. Direct experimental measurement of relative permeability for different types of soils has been performed. Mathematical approximations based on previous experiments are generally preferred for estimating the relative permeability because of the difficulty in conducting direct experiments.

Various researchers have proposed correlations based on mathematically-derived relationships or experimental data to

predict the relative permeability [15]. Most of the existing relative permeability correlations are based on the following types of physical models: capillary model, statistical model, empirical model and network model [15]. Empirically-derived models based on direct experimental observation provide the most reasonable approximations due to their simplicity and reliance on direct measurements compared to other types of models [15]. Even though all of the above-mentioned models have been used to predict the relative permeability [16], they may not be appropriate for use in a fuel cell DM. Typically, the general shape of the relative permeability curves is estimated by the following equations [15]:

$$k_{r-nw} = A(s_{nw})^n \quad \text{and} \quad k_{r-w} = B(1 - s_{nw})^m \tag{11}$$

where A, B, n and m are constants depending upon the structure of the porous media.

In the present study, four well-established empirical correlations describing the water–air two-phase system (Wyllie model, Corey model, Brooks-Corey model and the Van-Genuchten model) are used to predict a representative non-wetting phase (liquid) relative permeability for differently engineered DMs, based on the experimental capillary pressure data provided by Ref. [10]. The relative permeability calculation in each model is based on the effective saturation (s_e), which requires the irreducible water saturation (s_{irr}) as an input. The irreducible saturation or immobile saturation, (s_{irr}), is the amount of trapped water in the pores of the DM. It can be considered as a threshold point below which liquid remains immobile.

$$s_e = \frac{s - s_{irr}}{1 - s_{irr}} \tag{12}$$

2.2.2. Wyllie model

Wyllie [14,15] suggested simple liquid–gas relative permeability equations for well and non-consolidated sands, based on the capillarity concept developed by Purcell [17] and Burdine [18]. The Wyllie approach is widely applied in fuel cell modeling studies due to its simplistic application [12].

$$k_{r-nw} = (s_{e-nw})^3 \qquad k_{r-w} = (1 - s_{e-nw})^3 \tag{13}$$

where s_e, nw and w represents the effective saturation, non-wetting phase and wetting phase, respectively.

2.2.3. Corey model

Purcell developed an analytical expression to compute the relative permeability from experimental capillary pressure data [16]. Burdine [18] introduced the tortuosity factor concept into the original capillary pressure model developed by Purcell [17]

and extended this equation to calculate the multiphase relative permeability. Corey combined these two approaches into a single form, based on the assumption that capillary curves over a certain range of saturations can be approximated using the linear expression, $1/P_c^2 = C \cdot s_{e-w}$, where C is a constant, and obtained the following relative permeability equations for non-wetting and wetting phases [15]:

$$k_{r-nw} = [1 - (s_{e-w})^2][1 - s_{e-w}]^2 \qquad k_{r-w} = (s_{e-w})^4. \tag{14}$$

2.2.4. Brooks-Corey model

Brooks and Corey modified the original Corey capillary pressure-saturation relationship to predict the relative permeability for any pore size distribution [15].

$$k_{r-nw} = (1 - s_{e-w})^2[1 - (s_{e-w})^{2+\lambda/\lambda}]$$
$$k_{r-w} = (s_{e-w})^{2+3\lambda/\lambda} \tag{15}$$

where λ is the pore size distribution index of the porous media, which is a specific characteristic of the pore size distribution, and it is typically determined by fitting the water retention data to the Brooks-Corey correlation.

2.2.5. Van Genuchten model

One of the most recent relative permeability correlations was proposed by Van Genuchten [19,20]. Van Genuchten derived an empirical correlation that accounts for variable pore size and connectivity concepts of the porous media. This model unites the entire range of saturation in a single curve, even though not all of the saturation regions (e.g., dry end, wet end) are governed by the same physics [19,20]. According to the Van Genuchten model, the relative permeability of the non-wetting and wetting phases can be calculated as follows:

$$k_{r-nw} = (1 - s_{e-w})^{1/3}[1 - (s_{e-w})^{1/m}]^{2m}$$
$$k_{r-w} = (s_{e-w})^{0.5}[1 - (1 - (s_{e-w})^{1/m})^m]^2 \tag{16}$$

where m is a fitting parameter and can be extrapolated from capillary pressure–saturation data. The models utilized in the present study are summarized in Table 1. In all these models, the capillary pressure and the relative permeability are coupled; thus, each model requires the knowledge of capillary pressure as a function of water saturation. However, the standard porosimetry technique is incapable of distinguishing the isolated pores [10], thus the capillary pressure data presented in Ref. [10] is associated with the total saturation. Therefore, a lower limit value of s_{irr}, 0.05, is used in the present study, assuming all the pores are almost connected, to minimize the isolated pore

Table 1
Summary of relative permeability models utilized in this study

Models	Relative permeability (non-wetting phase)	Relative permeability (wetting phase)
Wyllie model	$k_{r-nw} = (s_{e-nw})^3$	$k_{r-w} = (1 - s_{e-nw})^3$
Corey model	$k_{r-nw} = [1 - (s_{e-w})^2][1 - s_{e-w}]^2$	$k_{r-w} = (s_{e-w})^4$
Brooks-Corey model	$k_{r-nw} = (1 - s_{e-w})^2[1 - (s_{e-w})^{2+\lambda/\lambda}]$	$k_{r-w} = (s_{e-w})^{2+3\lambda/\lambda}$
Van Genuchten model	$k_{r-nw} = (1 - s_{e-w})^{1/3}[1 - (s_{e-w})^{1/m}]^{2m}$	$k_{r-w} = (s_{e-w})^{0.5}[1 - (1 - (s_{e-w})^{1/m})^m]^2$

s_e represents the effective saturation.

Table 2
Material properties of the tested DMs adapted from Ref. [10]

Material	Type	Thickness (μm)	PTFE (wt.%)	Hydrophilic porosity	Total porosity
SGL 10BA	Paper	380	5	0.63	0.91
SGL 10BB	Paper w/MPL	420	5	0.45	0.87
Toray 090	Paper	190	0	0.63	0.79
E-Tek Cloth	Cloth	350	0	0.74	0.72

size effect and estimate the bulk multi-phase connectivity of a typical fuel cell DM.

2.2.6. Empirical fit

The capillary pressure–saturation curves obtained by Gostick et al. [10] were used as benchmark data to obtain a polynomial fit explicitly relating the P_C versus s_l for the tested fuel cell DMs under a limited set of conditions. Four different types of diffusion media including: *SGL 10BA*, *SGL 10BB*, *Toray 090* and *E-TEK Cloth A*, were selected, and the material properties of these DMs including the total and hydrophilic porosities are tabulated in Table 2 (adapted from Ref. [10]).

Fig. 4a depicts the measurements of capillary pressure–saturation (provided by Ref. [10]) for the DM chosen in this study. As seen in Fig. 4a, the measured capillary

pressure for all DM samples follows the same qualitative trend, even approaching similar capillary pressures especially at low saturations ($s_{nw} < 0.6$). The difference in capillary pressure can be attributed to the differences in the specific morphological and characteristics and PTFE loading of the chosen DMs. As also stated in Ref. [10], a sudden increase in capillary pressure is observed after the threshold saturation value of 0.8. The sudden change in the measured data at high saturation values ($s_{nw} > 0.8$) causes a significant amount of scattering, which in turn, complicates the representation by an accurate curve-fit. Typically, a fuel cell operates in a saturation range of 0–0.6, therefore the capillary pressure measurements within the saturation range of 0–0.8 were considered to be appropriate benchmark data. A single equation representing the actual $P_C - s_l$ relation of the tested DMs (Eq. (17)) was deduced based on the best fit of the data ($0 < s_{nw} < 0.8$) and shown in Fig. 4b. Even though the empirical curve-fit starts to deviate from the actual data at high saturations ($s_{nw} > 0.8$) due to the sudden increase in the measured capillary pressure, the curve-fit reasonably predicts the measured data within the saturation range of 0–0.8 covering the range, in which a polymer electrolyte fuel cell typically operates.

$$P_C = -4854.1s_l^2 + 12958s_l \quad \text{(in Pa)} \quad R^2 = 0.80$$
$$0 < s_{nw} < 0.8 \qquad (17)$$

It is worthwhile emphasizing that Eq. (17) was utilized solely to evaluate the saturation predictions of the traditional Leverett approach equipped with *J*-function for the DM samples tested by Ref. [10]. Eq. (17), therefore, *should not be considered as a generalized relationship appropriate for all type for fuel cell DM*, although such a relationship is definitely required.

As expressed, capturing the myriad changes of the transport parameters within the pores of the DM is difficult due to the minute length scale and the complex heterogeneous nature of the DM structure. The distinctive feature of the presented empirical fit is that it implicitly accounts for the variations in the relevant transport properties of the tested DMs including porosity, surface tension and contact angle, since it relies on the actual experimental capillary pressure data of Ref. [10]. Therefore, such a representative curve-fit based on experimental measurement of the tested DM samples eliminates the requirement of porosity, surface tension and *J*-function as an input. In addition the contact angle parameter, which is a required input in Leverett approach, is implicitly embedded into the empirical curve-fit, thereby accounting for variations in internal contact angle caused by the anisotropic nature of the hydrophobic coating. This feature enables us to eliminate the need for the selection
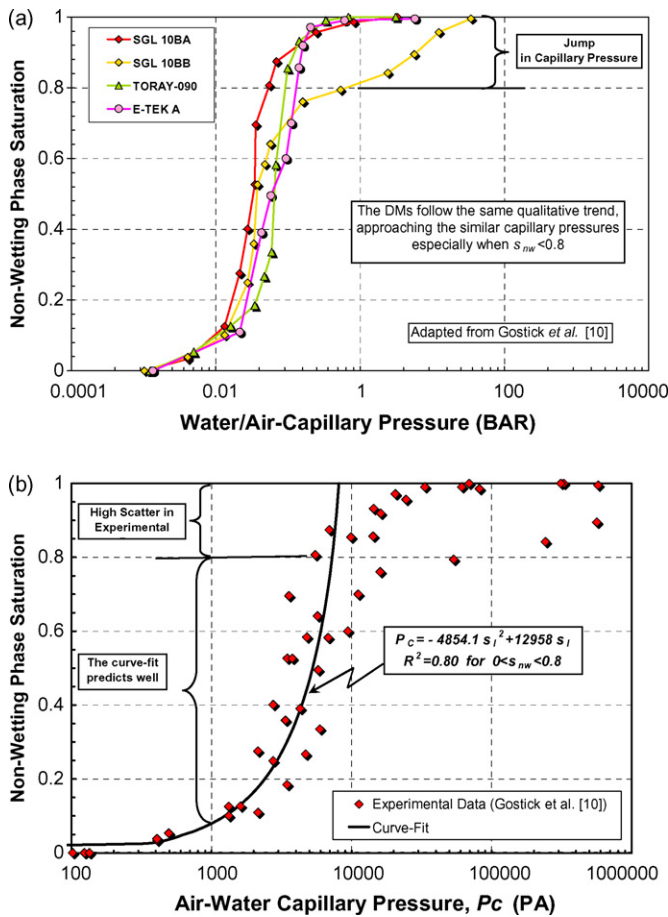
Fig. 4. (a) Measured capillary pressure–saturation data for tested DM samples (adapted from Gostick et al. [10]) and (b) comparison of the curve-fit and experimental data provided by Ref. [10].

of a single (and unrealistic) surface contact angle, *but* Eq. (17) *should not be considered as a generalized relationship appropriate for all types of fuel cell DM.*

3. Mapping the liquid saturation distribution

3.1. Modified constitutive relations

3.1.1. Characteristic relative permeability

A new characteristic relative permeability correlation appropriate for uncompressed room temperature thin-film fuel cell DM was obtained by compiling the experimental capillary pressure data presented in Ref. [10] to the empirical models described in Section 2.2. The relative permeability correlation obtained from these models was fit onto a single curve in the form of $k_{r-nw} = A(s_{e-nw})^m$ to represent the overall relative permeability behavior of the tested DMs. Eq. (18) shows the predicted relative permeability relation for DMs tested by Ref. [10] at room temperature and under no compression.

$$k_{r-nw} = (s_{nw})^{2.16} \qquad R^2 = 0.978 \qquad (18)$$

This relationship should be used with caution, as it is a bulk fit for the four different DMs tested by [10], under no compression at room temperature. Nevertheless, it is an improvement of the existing models applied without linkage to the measured experimental data.
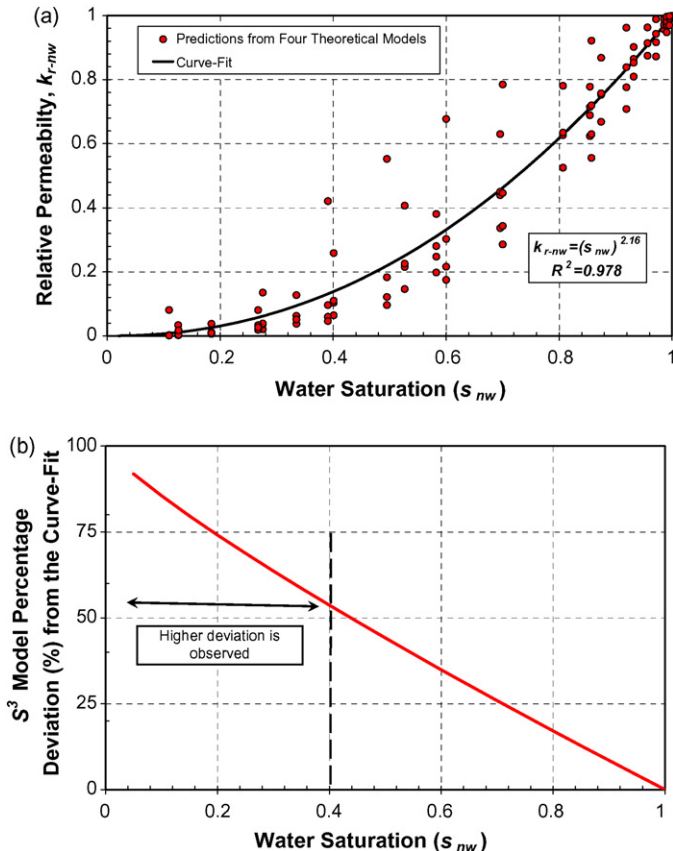

Fig. 5. (a) Predicted liquid relative permeability curve and (b) percentage deviation of the Wyllie model from the predicted curve-fit.

Fig. 5a depicts the predicted relative permeability curve as a function of liquid saturation. The predicted relative permeability curve for the non-wetting phase shows a modest increase at low saturations, because at low saturations only a small portion of the pores are occupied by the liquid water, whereas a large portion of the pores are still available for the gas-phase transport. Hence, there is no significant impact of saturation on the reactant flow. However, at high saturations, the predicted relative permeability exhibits a considerable increase with small increases in saturation, because as the available pores are nearly all filled by the liquid water and gas-phase transport is highly restricted.

Fig. 5b shows the percentage deviation of the typically used Wyllie model (s^3 model) from the predicted curve-fit at different saturation values. When the present prediction is compared with the commonly used Wyllie model ($k_{r-nw} = (s_{nw})^3$) over the entire spectrum of water saturation ($0 < s_{nw} < 1$), a significant difference between the predicted relative permeability values is observed, especially at low water saturation values ($s_{nw} < 0.4$). The discrepancy between the predictions diminishes at relatively higher saturation values ($s_{nw} > 0.6$). Physically speaking, the coefficients in Wyllie model were generated for non-consolidated sands. Thus, the applicability of the Wyllie model by itself may not accurately describe the relative permeability of the fuel cell DM. Currently, the presented approach (Eq. (18)) takes into account a broader range of theoretical analysis of relative permeability in porous media with the intent of providing an improved relative permeability relation and it incorporates direct experimental data obtained in Ref. [10] for various common DMs. However, the *direct measurement* of relative permeability for thin fuel cell DM as a function of temperature, compression and PTFE content is still needed to verify the applicability of present prediction.

3.2. Implementation of different constitutive relations

Different constitutive relations were implemented within the theoretical model described in Section 2.1 to predict the local liquid saturation profiles. The local saturation profiles were predicted for two different cases (Case 1 and Case 2 as described below), governed by different relations. Furthermore, operational conditions and relevant structural properties of thin-film porous DM, including net water transport coefficient, current density, thickness and hydrophobicity, were examined for these two cases in order to capture the significance of the differences in liquid saturation profiles.

In Case 1, the standard Leverett function and Wyllie relative permeability relation ($k_{r-nw} = s_{nw}^3$) were used in Eq. (9), whereas in Case 2, along with the modified relative permeability ($k_{r-nw} = s_{nw}^{2.16}$), an empirical curve-fit (Eq. (17)) representing the measured $P_C - s_l$ relation of the DMs tested by Ref. [10] was directly integrated into the theoretical model. The relations used in each case and the final form of the governing equations for these two cases are shown in Table 3.

Analytical solution of the equations in Table 3 enables determination of the local saturation, s_l, at any location, x, of the DM. The final form of the governing liquid transport equations overall include a number of engineering parameters, including the

Table 3
The constitutive relations used and the final form of the governing equations for Case 1 and Case 2

| | Constitutive relations | |
	Capillary pressure–saturation relationship	Relative permeability
Case 1	$P_C = \gamma \cos\theta \left(\frac{\varepsilon}{k}\right)^{1/2} J(s_l)$	Wyllie model
Standard Leverett function	$J(s_l) = 1.417s_l - 2.120s_l^2 + 1.263s_l^3$	$k_{r-nw} = s_{nw}^3$
Case 2	$P_C = -4854.1s_l^2 + 12958s_l$	Present model
Empirical fit	$(0 < s_{nw} < 0.8)\ R^2 = 0.80$ (in Pascals)	$k_{r-nw} = s_{nw}^{2.16}$
	Final governing equations (Eq. (9))	
Case 1	$-\frac{I(2\alpha+1)\mathrm{MW}^{H_2O}\nu_l}{2F\gamma\cos\theta\sqrt{k\varepsilon}}(x) = 0.354s_l^4 - 0.848s_l^5 + 0.630s_l^6$	
Case 2	$-\frac{I(2\alpha+1)\mathrm{MW}^{H_2O}\nu_l}{2Fk}(x) = 4100.6s_l^{3.16} - 2333.7s_l^{4.16}$	

porosity of the DM, permeability, current density, contact angle, surface tension (function of temperature), net water transport coefficient and liquid saturation.

3.3. Validation of the empirical curve-fit

To evaluate the accuracy of the empirically derived curve-fit (Eq. (17)), an additional assessment was performed. The saturation prediction of Eq. (17) was compared with the saturation profiles predicted by the measured capillary pressure–saturation curves of the tested DM samples [10]. The capillary pressure–saturation curve of each DM was separately implemented into the analytical framework and the corresponding saturation profiles were calculated at 1 A cm^{-2}, assuming a typical DM thickness of 300 μm. Fig. 6 presents the predicted saturation profiles of Case 2 by implementing the measured capillary pressure–saturation curves of *SGL 10BA*, *SGL 10BB*, *TORAY 090*, *ETEK-A* and the curve-fit given in Eq. (17). The saturation profiles over the entire thickness appear to follow similar qualitative trend, predicting very close saturation values. More importantly, the curve-fit given in Eq. (17) is observed to reasonably well-predict the saturation values for all DM samples, with an uncertainly of ±6.8%, strongly supporting

the effectiveness and applicability of this approach for comparing the experimental data with the prediction of Leverett approach.

In addition, the small deviation between the saturation predictions indicates that even though the change in PTFE content may affect the transport parameters, within the context of the experimental data provided for the tested DM materials, the predicted saturation values appear to be relatively insensitive to the change in PTFE within the specified range of DM samples (from 0 to 5 wt.% PTFE).

4. Results and discussions

4.1. Effects of DM properties

The theoretical model was solved to predict the liquid saturation profiles for different thicknesses and various hydrophobicity levels. The predicted saturation profiles corresponding to different DM thicknesses were compared. However, the effect of hydrophobicity on the predicted local saturations was only performed for Case 1, since Case 2 is a curve fit for four different DMs tailored with similar PTFE content (ranging from 0 to 5 wt.%) and the contact angle parameter is implicitly embedded into this empirical fit, thus not required as an input. The liquid saturation was set to zero at the DM-flow channel interface as a boundary condition, representing a drainage condition. The condition of zero liquid surface coverage in the flow channel by liquid water is reasonably valid for carbon cloth and conditionally expected for carbon paper DM under large air stoichiometry [6].

4.1.1. DM hydrophobicity

As expected, the hydrophobicity of the DM has a strong impact on the liquid saturation distribution predicted by the Leverett approach. The liquid saturation profiles for different contact angle values were determined for Case 1 and shown in Fig. 7a. At any specified location, the maximum liquid saturation is predicted for contact angle 95°, whereas the minimum local saturation occurred for contact angle 150°. In addition, for a constant fractional distance from the catalyst layer, the theoretical model was solved for Case 1 to predict the local saturation values as a function of contact angle values (shown in Fig. 7b). As
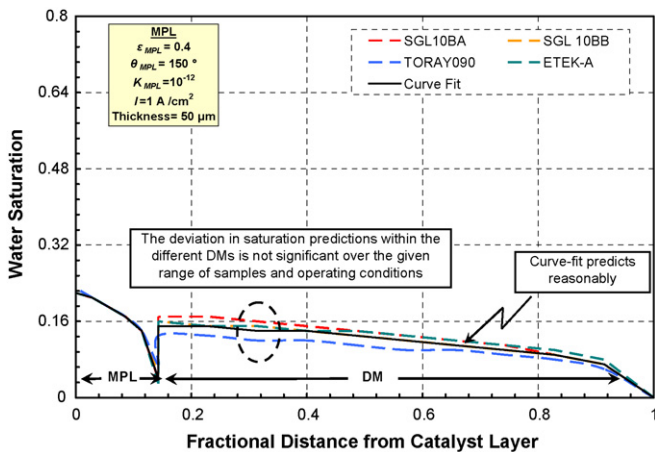

Fig. 6. Predicted saturation profiles for Case 2 (using empirical curve-fit) implementing the individual measured capillary pressure curves for all DM samples and the curve-fit presented in Eq. (17).

Fig. 8. Predicted saturation profiles for Case 1 (using standard Leverett approach) and Case 2 (using empirical curve-fit) for different DM thicknesses.
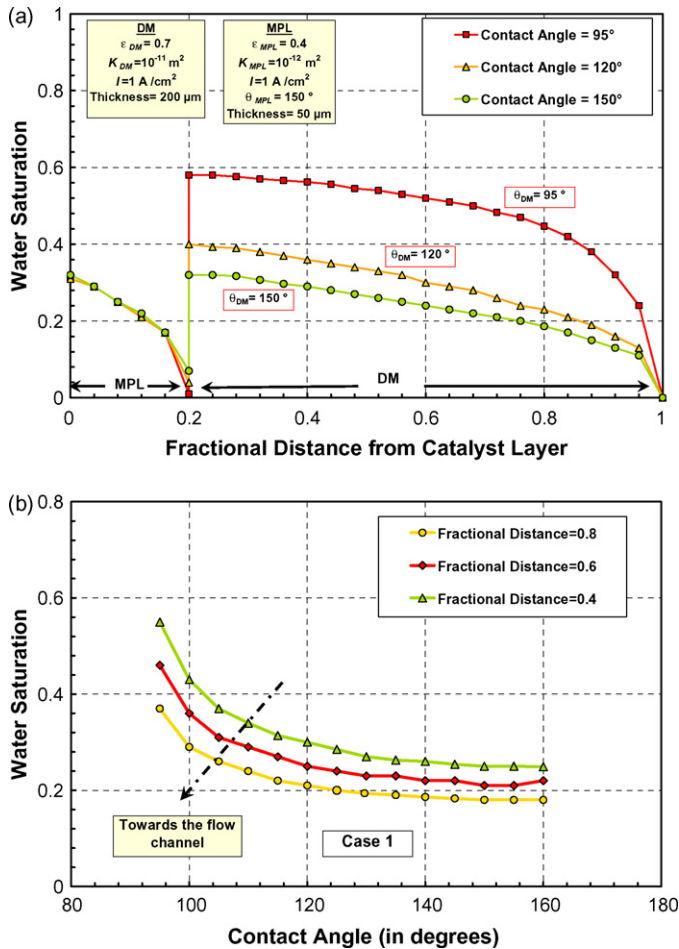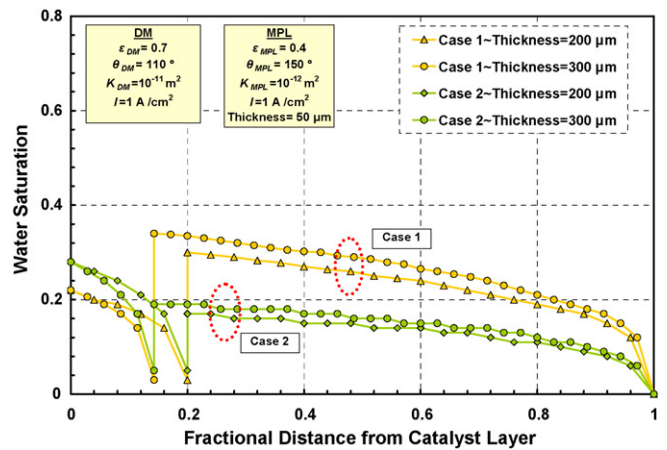
Fig. 7. (a) Predicted saturation profiles of Case 1 (using standard Leverett approach) for different contact angle values and (b) saturation predictions of Case 1 (using standard Leverett approach) at various locations for different contact angle values.

the contact angle increases from 95° to 110°, a relatively severe decrease in local saturation values is observed. Above 90°, the liquid water transport is enhanced noticeably by an increase in hydrophobicity, but with diminishing dependence. Physically, the surface adhesion force in carbon fibers is reduced by rendering the DM surface more hydrophobic, causing higher surface contact angle. As a result, at higher PTFE loadings of the DM, the liquid water molecules on high PTFE loading fibers tend to be more unstable, enabling enhanced liquid transport through the pores of the DM.

4.1.2. DM thickness

Fig. 8 presents the predicted saturation profiles of Case 1 and 2 for two different DM thicknesses (200 and 300 μm). All cases (Case 1 and 2) demonstrate the same qualitative trend, but predict lower saturation values for thinner DM at any specified location. Physically, for a thinner DM, the liquid water concentration gradient becomes larger, causing a higher driving force, which in turns facilitates the liquid transport. Any decrease in DM thickness shortens the path length of the liquid water, thus reducing the liquid transport resistance. Therefore, a smaller liquid saturation difference becomes sufficient to drive the liquid

water from higher saturation region to lower saturation region for a thin DM.

In terms of saturation predictions of these two Cases (Case 1 and 2), it can be observed from Fig. 8 that while the cases follow the same qualitative trend, the predicted saturation values differ significantly as a function of constitutive relation. While the capillary-induced transport is defined by Leverett approach in Case 1, the discrepancy in saturation predictions between Case 1 and 2 is noticeable at each location. In Case 1, the standard Leverett function ($J(s_l)$) is used, however, in Case 2, a polynomial fit purely derived from experimental data of Ref. [10] has been employed. The difference in predicted saturation values between each case is relatively more pronounced, even reaching a peak value of 0.13 at the MPL interface, as shown in Fig. 8.

This vast difference in predicted saturation values indicates that the standard Leverett function fails to accurately describe the capillary transport behavior of the fuel cell DM. This noticeable difference can be attributed to the fact that the actual $P_C - s_l$ relation is *directly* input into the liquid transport model in Case 2. The fuel cell DM has a *mixed wettability* network, while the Leverett approach integrates a constant porosity and a representative surface contact angle (uniform wettability), which is not the case in fuel cell DM. The discrepancy in the model outputs brings into question of the appropriateness of assuming constant values for porosity and contact angle. An improved approach would not only include the rigorous interaction of effective porosity and liquid saturation, but would also include the effects of compressibility, temperature and the *mixed wettability* (non-uniform contact angle) as well.

Significant structural complexity in the DM leads to difficulty in defining a meaningful internal contact angle parameter. The wettability on any surface can be characterized in terms of contact angle, which is closely related to the molecular interaction of matters at the contact interface [11,22]. To date, empirical studies have been inconclusive regarding the representative average internal contact angle at the microscopic level. Due to experimental limitations at the pore-level, external contact angle measurements are commonly employed to estimate the internal contact angle, and it is doubtful that an aver-

age contact angle approach is appropriate since the connected hydrophilic/hydrophobic pores of the DM act in parallel. Moreover, external contact angle measurements fail to include the effects of the different levels of surface energy associated with the carbon fibers. Therefore, measured external contact angles may not reflect a statistical average of contact angles associated within the highly heterogeneous DM pores [23].

In addition, the standard Leverett function utilized in Case 1 accounts for the porous DM in terms of a single dry porosity value. However, the accumulation of liquid water into the available pores and associated change in effective porosity can lead to a substantial influence on transport properties of the DM [23–25]. Once the available pore space is occupied by the liquid water, the liquid flow path resistance increases. Therefore, selecting a representative value of DM porosity may fail to account for the liquid transport phenomena occurring in fuel cells.

4.2. Operating conditions

Optimization of the operating conditions is also of great importance for the avoidance of flooding problems in the DM. The level of liquid saturation in the cathode DM is strongly related to the operating current density and net water diffusion flux across the membrane [26–29]. The net water transfer coefficient, α, is strongly coupled with the current density, since the rate of water transport across the membrane *via* diffusion and electro-osmotic drag is proportional to the cell operating current density. This parameter can be influenced by the selection of DM and MPL properties. In the present model, current density and net water transfer coefficient are treated as independent parameters to distinguish the significance of each effect separately. The theoretical model (Eq. (9)) was solved for different current densities and net water transfer coefficients, while holding the other parameters constant. The predicted liquid saturation profiles were analyzed and compared. The boundary condition is again defined such that the liquid saturation is zero at the DM-flow channel interface.

4.2.1. Net water transfer coefficient

Fig. 9a shows the effect of net water transfer coefficient, α, on the liquid saturation profile for Case 1. As expected, the present model predicts higher liquid saturation in the cathode DM for the higher net water transfer coefficient ($\alpha = 0.1$ versus $\alpha = 1$). As the net water transfer rate increases, the cathode side becomes more prone to the accumulation of excess liquid water, which in turns, increases the local liquid saturation values in the cathode DM.

4.2.2. Operating current density

Fig. 9b shows the liquid saturation distribution for Case 1 under different operating current densities (0.2, 1 and 2 A cm^{-2}). At any specified location, the predicted saturation value is higher for the highest current density (2 A cm^{-2}), whereas the lowest liquid saturation is predicted for the lowest current density (0.2 A cm^{-2}), as expected [5]. The same behavior is also observed in the MPL.
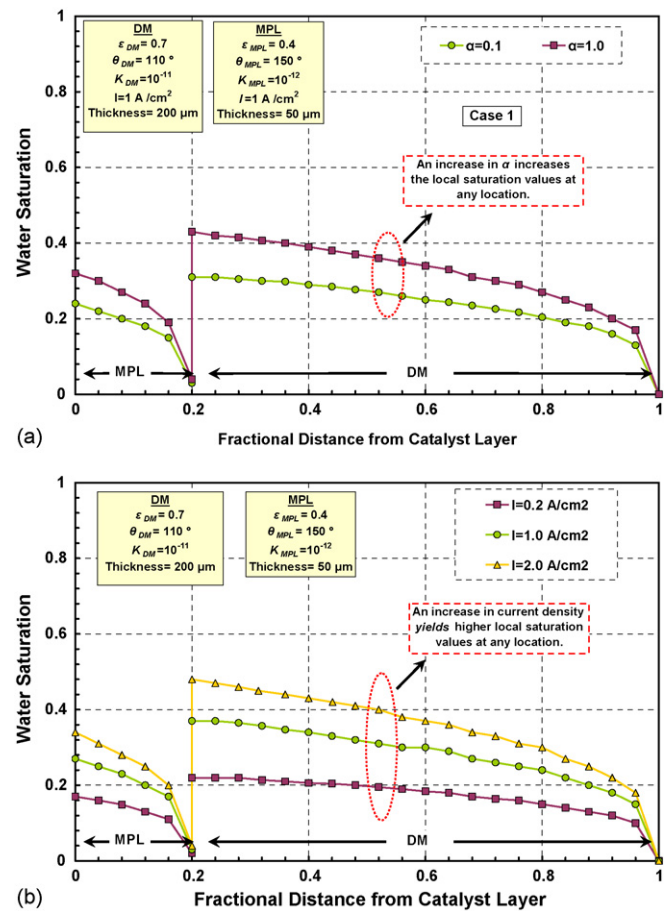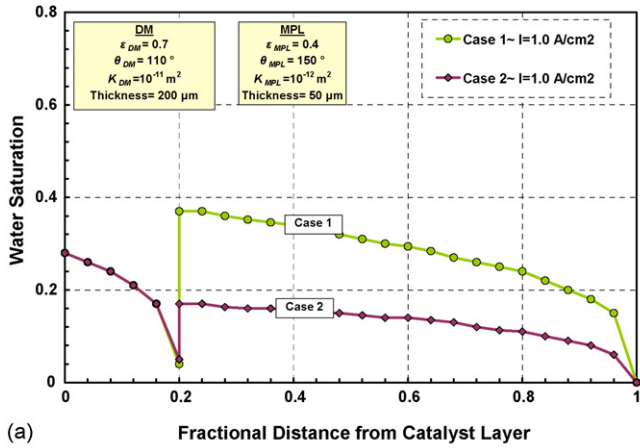

Fig. 9. Predicted liquid saturation profiles for Case 1 (using standard Leverett approach); (a) for different net water transfer coefficients, (b) under different current densities.

The saturation profiles predicted by the model for Case 1 and 2 are compared for a current density of 0.2 A cm^{-2} and α value of 0.5 in Fig. 10. As previously discussed, the origin of the considerable difference in predicted saturation values arises from employing standard Leverett function in Case 1, which assumes a constant porosity and contact angle. However, Case 2 is represented by an experimental P_C–s_l curve, which implicitly accounts for the variation of DM structural properties such as internal contact angle and effective porosity. This remarkable deviation in the predicted local saturation values between Case 1 and 2 further demonstrates the inapplicability of using the standard Leverett approach.

4.3. Case sensitivity analysis

A sensitivity analysis was performed to ascertain how each specified case prediction depends upon the DM thickness, the net water transfer coefficient and the current density, and to assess the range over which the model predictions become sensitive to changes in these parameters.

As a first step, the functional dependence of the liquid saturation as a function of a chosen input parameter was determined at a specified location (e.g. a fractional distance from the catalyst layer of 0.8). Then the derivative of this function with respect to
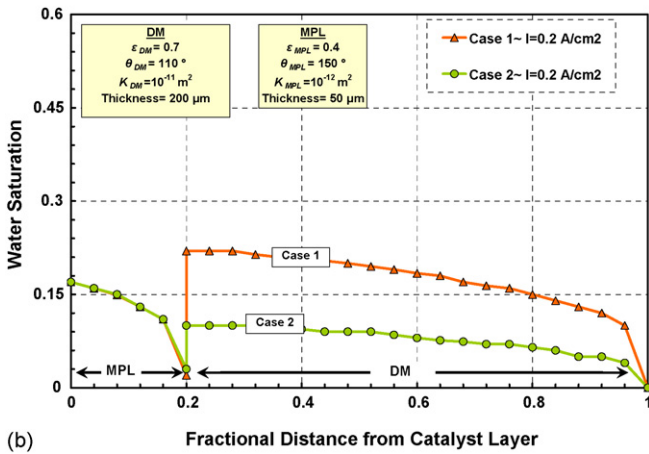
Fig. 10. Predicted saturation profiles for Case 1 (using standard Leverett approach) and Case 2 (using empirical curve-fit) for 200 μm DM and α value of 0.5; (a) at current density $1.0\,\mathrm{A\,cm^{-2}}$, (b) at current density $0.2\,\mathrm{A\,cm^{-2}}$.

Fig. 11. (a) Predicted saturation profiles for Case 1 (using standard Leverett approach) and Case 2 (using empirical curve-fit) for different DM thicknesses, (b) rate of change of saturation predictions for the two cases with varying DM thickness.

the chosen input parameter was computed to evaluate the sensitivity of the model prediction corresponding to any change in that input parameter. A greater slope implies a greater sensitivity, as shown in Eq. (19). The derivatives with respect to the specified inputs are also compared between Case 1 and Case 2.

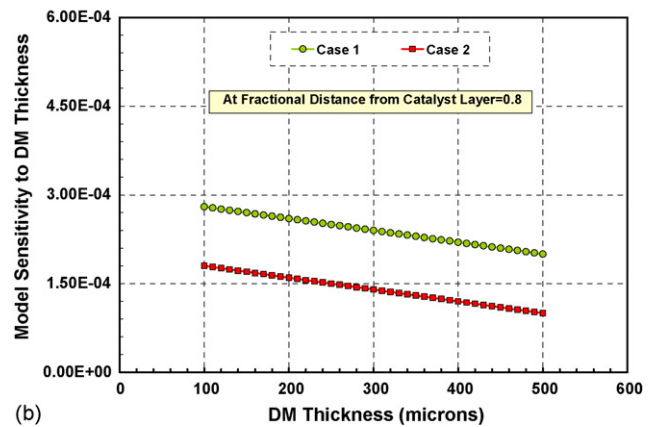$$(s_1)_{\text{Case-}j} = \text{Func}(X) \quad \text{at a specified location}$$

$$\left(\frac{\partial s_1}{\partial X}\right)_{\text{Case-}j} > \left(\frac{\partial s_1}{\partial X}\right)_{\text{Case-}i}$$

$$\Rightarrow \text{Case-}j \text{ is more sensitive than Case-}i. \qquad (19)$$

The first investigated input parameter is the DM thickness. Fig. 11a depicts the predicted saturation profiles for two different DM thicknesses. As the DM thickness increases from 200 to 300 μm, the predicted saturation values at each location increases for all cases. It is observed that the average percentage increase in predicted saturation values as the thickness is increased from 200 to 300 μm is found to be 10.3% for Case 1 and 10.5% for Case 2, approximately equal. The sensitivity of the case predictions corresponding to any change in DM thickness was also investigated at a fractional distance from catalyst layer of 0.8. Fig. 11b shows the rate of change of the predicted

saturation values corresponding to the DM thicknesses from 100 to 500 μm. As seen from the graph, the magnitudes of the slopes are on the order of 10^{-4}, meaning that DM thickness seems to have minor effect on case predictions.

A case sensitivity analysis of the net water transfer coefficient was also performed. Two different values of net water transfer coefficient ($\alpha = 0.1$ and 1.0) were implemented and the predicted saturation profiles are shown for Case 1 and 2 in Fig. 12a. The increase in net water transfer coefficient from 0.1 to 1 appears to cause a slight increase in the predicted saturation values. However, the amount of increase is different for Case 1 and 2. In order to identify the relative significance of changing the net water transfer coefficient on case predictions, the sensitivity analysis was performed at a specified location (a fractional distance from the catalyst layer of 0.8). Fig. 12b depicts that the sensitivity of the each case is reduced as the net water transfer coefficient increases from 0.1 to 0.5 and then starts to increase as the net water transfer coefficient increases from 0.5 to 1.0. As seen from Fig. 12b, Case 2 exhibits relatively smaller slope change, ranging from 0.013 to 0.085, whereas Case 1 has higher slope values (varies from 0.03 to 0.2) over the entire net water transfer coefficient, meaning that model predictions for Case 1 is relatively more sensitive, (by an average factor of 2.2) than that of Case 2.
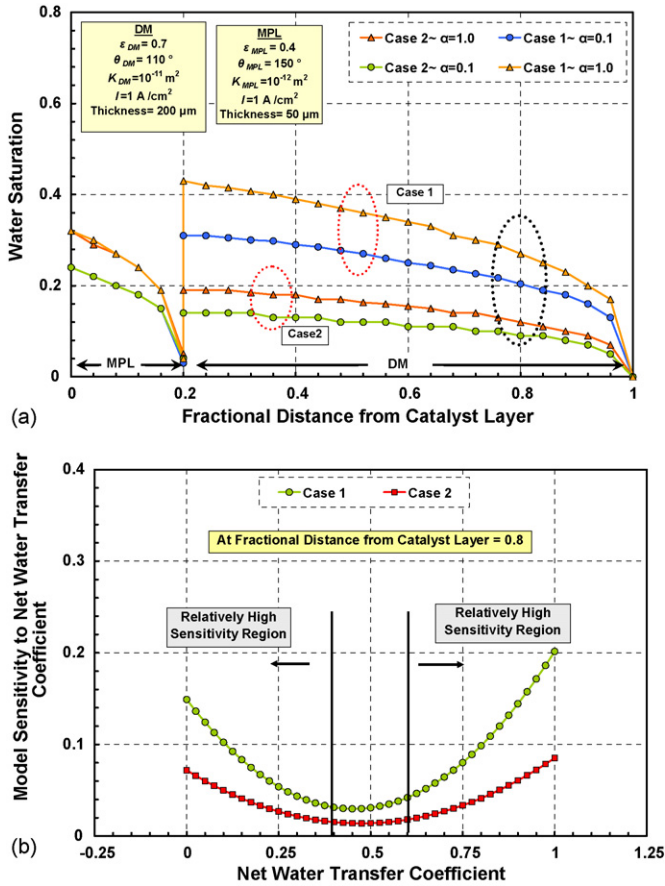
Fig. 12. (a) Predicted saturation profiles using Case 1 (using standard Leverett approach) and Case 2 (using empirical curve-fit) for different net water transfer coefficients, (b) rate of change of saturation predictions for all cases with varying net water transfer coefficients.
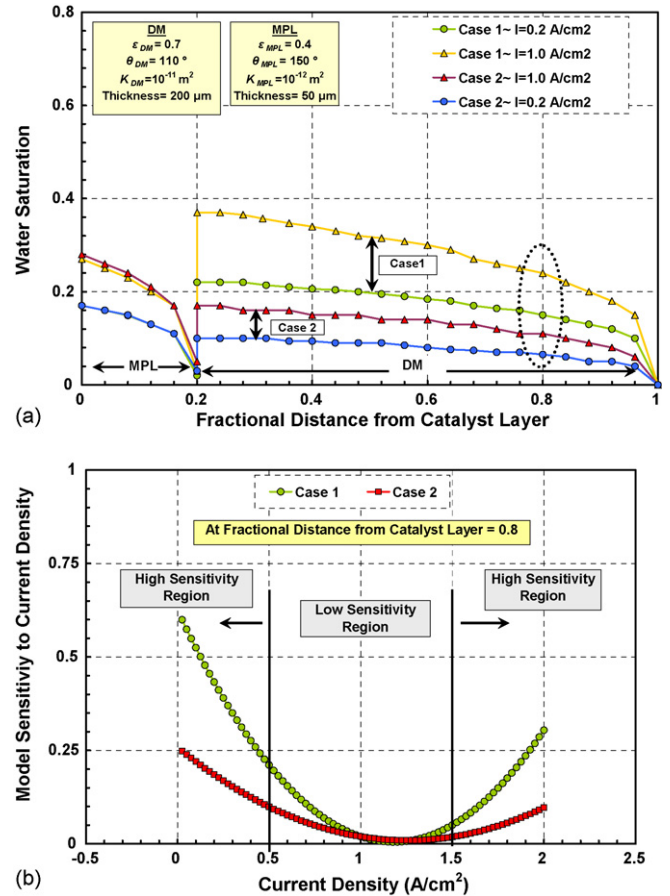

Fig. 13. (a) Predicted saturation profiles using Case 1 (using standard Leverett approach) and Case 2 (using empirical curve-fit) under different current density, (b) rate of change of saturation predictions for all cases under various operating current densities.

The final investigated input parameter is current density. Two different operating current densities ($I = 0.2$ and $1.0\,\mathrm{A\,cm^{-2}}$) were implemented in two cases and the behavior of the model predictions were analyzed. Fig. 13a shows the predicted liquid saturation distribution for Case 1 and 2 under different current densities. As expected, the increase in current density gives rise to the predicted saturation values at each location due to the enhanced water generation. However, when the amount of average increase in predicted saturations is compared, Case 1 exhibits relatively smaller percentage increase (59%) compared to Case 2 (65%), in response to the change in current density. Fig. 13b depicts the rate of change of the predicted saturation values as a function of current density at a specified location (a fractional distance from catalyst layer of 0.8). As seen from Fig. 13b, Case 1 is observed to be more sensitive compared to Case 2 with an average factor of 2.08, corresponding to any changes in current density over the range of $I = 0\text{–}2\,\mathrm{A\,cm^{-2}}$. The sensitivity is more pronounced for these two cases when the current density varies from 0 to $0.5\,\mathrm{A\,cm^{-2}}$ and from 1.5 to $2\,\mathrm{A\,cm^{-2}}$. Conversely, the predicted sensitivity for all cases becomes relatively small when the current density is in the range of $0.5 < I < 1.5\,\mathrm{A\,cm^{-2}}$.

The magnitude of the slope with respect to any specified input parameter can be used to compare the relative significance of each input parameters on the model prediction. Among the input parameters of concern (thickness, current density and net water transfer coefficient), the current density seems to be the most crucial input parameter for both Case 1 and Case 2, when the magnitude of the rate of change is compared between the each input parameters. Based on these analyses, it can be concluded that the model prediction for all cases is relatively more sensitive to any change in current density rather than the changes in the DM thickness and net water transfer coefficient.

5. Conclusions

The effectiveness of the traditional Leverett approach (equipped with J-function) to describe the capillary-induced flow in thin-film fuel cell DM was investigated. An empirical polynomial fit (P_C–s_l) describing the capillary pressure–saturation relation of the DMs listed in Table 2 was derived based on the experimental capillary pressure–saturation curves provided by Ref. [10]. In addition, a new representative relative permeability correlation ($k_{r-nw} = s_{nw}^{2.16}$) compiling a broader range of theoretical basis for the tested fuel cell media by Ref. [10] was obtained. These correlations, along with the Leverett approach equipped with J-function, were integrated into an analytical framework to predict liquid saturation pro-

files for differently engineered DMs under various operating conditions. The variations in liquid saturation predictions associated with employing different correlations were assessed and the effectiveness of the traditionally used Leverett function was determined to be poor.

The Leverett approach consistently over-predicts the DM saturation values compared to the ones obtained with the empirical fit of the experimental data. The significant variation in the predicted saturation profiles suggests that using the traditional Leverett approach is indeed inadequate to describe the capillary transport characteristic of a fuel cell DM, indicating the need to develop a modified approach appropriate for thin-film fuel cell media with *mixed wettability*. Finally, a sensitivity analysis was performed to ascertain how each specified correlations prediction depends upon the different input parameters. The model predictions are found to be relatively more sensitive to any change in current density rather than the changes in the DM thickness and net water transfer coefficient over the range of values tested.

Note that the presented correlations were generated based on the data [10] for a set of DMs tailored with PTFE ranging from 0 to 5 wt.% at room temperature under no compression. However, hydrophobicity of the DM, along with the operational environments such as temperature and compression needs to be investigated in a broader range to further isolate the effects of these parameters on the capillary transport characteristics of a fuel cell DM.

Acknowledgements

References

[1] Q. Dong, M.M. Mench, S. Cleghorn, U. Beuscher, J. Electrochem. Soc. 152 (2005) 2114.
[2] J.J. Kowal, A. Turhan, K. Heller, J. Brenizer, M.M. Mench, J. Electrochem. Soc. 153 (2006) 1971.
[3] A.Z. Weber, J. Newman, Chem. Rev. 104 (2004) 4679.
[4] J. Chen, T. Matsuura, M. Hori, J. Power Sources 131 (2004) 155.
[5] C.Y. Wang, Handbook of Fuel Cells—Fundamentals, Technology and Applications, John Wiley & Sons, Ltd., 2003, Chapter 29.
[6] U. Pasaogullari, C.Y. Wang, J. Electrochem. Soc. 151 (2004) 399.
[7] U. Pasaogullari, C.Y. Wang, K.S. Chen, J. Electrochem. Soc. 152 (2005) 1574.
[8] A.Z. Weber, J. Newman, Int. Commun. Heat Mass Transfer 32 (2005) 855.
[9] R. Bradean, K. Promislow, B. Wetton, Proceedings of American Society of Mechanical Engineers, vol. 375, Anaheim, CA, USA, 2004, p. 441.
[10] J.T. Gostick, M.W. Fowler, M.A. Ioannidis, M.D. Pritzker, Y.M. Volfkovich, A. Sakars, J. Power Sources 156 (2006) 375.
[11] E.C. Kumbur, K.V. Sharp, M.M. Mench, J. Power Sources 161 (2006) 333.
[12] B. Suden, M. Faghri, Transport Phenomena in Fuel Cells, first ed., WIT Press, UK, 2006, Chapter 5.
[13] J. Bear, Dynamics of Fluids in Porous Media, Dover Publications Inc., New York, NY, 1972.
[14] T.A. Corey, Mechanics of Immiscible Fluids in Porous Media, first ed., Water Resource Publications, Colorado, 1994, Chapter 2 and 3.
[15] M. Honarpour, L. Koederitz, A.H. Harvey, Relative Permeability of Petroleum Reservoirs, first ed., CRC Press, 1986, Chapter 2.
[16] K. Li, R.N. Horne, Water Resour. 42 (2006) 6405.
[17] W.R. Purcell, Am. Instit. Mining Metall. Eng.—J. Petroleum Technol. 1 (1949) 39.
[18] N.T. Burdine, J. Petroleum Technol. 5 (1953) 71.
[19] M.T. Van Genuchten, Soil Sci. Soc. Am. J. 44 (1980) 892.
[20] J.B. Kool, J.C. Parker, M.T. Van Genuchten, J. Hydrol. 91 (1987) 255.
[21] M.C. Leverett, Am. Instit. Mining Metall. Engineers—Petroleum Dev. Technol. 142 (1941) 152.
[22] J.G. Pharoah, K. Karan, W. Sun, J. Power Sources 161 (2006) 214.
[23] V. Gurau, M.J. Bluemle, E.S. De Castro, Y.-M. Tsou, J.A. Mann, T.A. Zawodzinski Jr., J. Power Sources 160 (2006) 1156.
[24] R. Roshandel, B. Farhanieh, E. Saievar-Iranizad, Renewable Energy 30 (2005) 1557.
[25] Z. Zhan, J. Xiao, D. Li, M. Pan, R. Yuan, J. Power Sources 160 (2006) 1041.
[26] D. Natarajan, T. Van Nguyen, J. Power Sources 115 (2003) 66.
[27] L. You, H. Liu, J. Power Sources 155 (2006) 219.
[28] S. Litster, D. Sinton, N. Djilali, J. Power Sources 154 (2006) 95.
[29] Q. Dong, Ph. D. Thesis, The Pennsylvania State University, 2006.